Convective activity in Mato Grosso state (Brazil) from microwave satellite observations: Comparisons between AMSU and TRMM datasets

Beatriz M. Funatsu, Vincent Dubreuil, Chantal Claud, Damien Arvor, Manoel
A. Gan

HAL is a multi-disciplinary open access archive for the deposit and dissemination of scientific research documents, whether they are published or not. The documents may come from teaching and research institutions in France or abroad, or from public or private research centers.

L'archive ouverte pluridisciplinaire **HAL**, est destinée au dépôt et à la diffusion de documents scientifiques de niveau recherche, publiés ou non, émanant des établissements d'enseignement et de recherche français ou étrangers, des laboratoires publics ou privés.

Convective activity in Mato Grosso state (Brazil) from microwave satellite observations: Comparisons between AMSU and TRMM data sets

Beatriz M. Funatsu,[1,2] Vincent Dubreuil,[2] Chantal Claud,[3] Damien Arvor,[4] and Manoel A. Gan[5]

[1]   We present a characterization of convective activity at sub-regional scale from two sets of satellite-based microwave observations: the Advanced Microwave Sounding Unit (AMSU) and the combined Tropical Rainfall Measuring Mission (TRMM) microwave imager and precipitation radar data, for the period 2001 to 2011. We focus on the state of Mato Grosso, Brazil, located at the southern edge of the so-called "Legal Amazon" which has undergone intense land cover transformation in the last 4 decades. The annual cycle of mean convective activity described by AMSU and TRMM are in good agreement, with a correlation close to 0.80. The mean amplitude of convective activity is maximal early in the rainy season, except for AMSU deep convective area, which presents a maximum in January. The diurnal cycle of convection was examined for the period 2003 to 2007, and it was found that convection is maximal near 1500 local time (LT) and minimal around 0700 LT. Unlike the amplitude, the phase shows little intraseasonal and interannual variability. A slight decrease in convective activity in the studied period was found, possibly indicating an extension of the dry season. Comparisons of convective activity between deforested and forested areas showed no significant differences in the phase of the diurnal cycle, but our analysis shows a tendency for increase (decrease) in convection in deforested (forested) areas for the period considered. A longer time series is however necessary in order to strengthen the robustness of our results.

1. Introduction

[2]   Convection is a ubiquitous feature of the tropical region, and is important for the heat transport from the lower troposphere to higher levels. Deep convection redistributes trace gases in the troposphere [*Wang and Chang*, 1993; *Hauf et al.*, 1995] and also carries atmospheric constituents from the troposphere into the tropical tropopause layer [*Holton et al.*, 1995; *Dessler*, 2002; *Wang et al.*, 2009; *Nielsen et al.*, 2011]. In the South American region, convection over the Amazon basin helps maintaining a climatological upper-level large-scale circulation known as the Bolivian high [*Virji*, 1981; *Lenters and Cook*, 1997], which is intimately related to other features of the South American climate [*Kousky and Kagano*, 1981; *Nishizawa and Tanaka*, 1983; *Horel et al.*, 1989]. Convection and related precipitation patterns in the Amazon region are affected by both global scale phenomena, such as the El Niño–Southern Oscillation in the tropical Pacific, and local forcing, such as fire and deforestation [*Aceituno*, 1988; *Lin et al.*, 2006; *Koren et al.*, 2008]. Although sea surface temperature alone cannot explain the low-frequency variability of rainfall in the Amazon [*Wang et al.*, 2011] large and local scale forcings can act in synergy to intensify the frequency of rainfall anomalies [*Lee et al.*, 2011]. Changes in precipitation patterns may in turn have an important role in the regional climate [*Malhi et al.*, 2008], and important ecological and socio-economic impact. Therefore, it is necessary to efficiently monitor convection as an indicator of climate change.

[3]   Satellite data is an essential source for studying precipitation and convection in the tropics since ground stations are often sparse and have discontinuous time series. The

[1]Laboratoire Atmosphères, Milieux, Observations Spatiales, CNRS, UMR 8190, IPSL, OVSQ, Guyancourt, France.
[2]Laboratoire COSTEL, UMR 6554, LETG, Université Rennes 2, Rennes, France.
[3]Laboratoire de Météorologie Dynamique, CNRS, UMR 8539, Ecole Polytechnique, Palaiseau, France.
[4]IRD, UMR, ESPACE DEV 228, INPE/CRA, Belém, Brazil.
[5]Brazilian National Institute for Space Research, Sao José dos Campos, Brazil.

Corresponding author: B. M. Funatsu, Laboratoire Atmosphères, Milieux, Observations Spatiales, 11 Boulevard D'Alembert, FR-78280 Guyancourt, France. (funatsu@latmos.ipsl.fr)

main sources of satellite data for such studies are based on infrared or microwave emissions. Microwave has the advantage that it can penetrate non-precipitating clouds and therefore provides three-dimensional information on cloud structure, in contrast with infrared data which gives information mainly on cloud top (temperature and pressure). Moreover, the description of the diurnal cycle of precipitation with infrared has shown poor correlation between these parameters [*Arkin and Meisner*, 1987]. In addition, a lag of around 3 to 4 h between precipitation estimates based on infrared data compared to ground based radar and rain gauges has been found, likely due to problems related to cirrus anvils identification with infrared [*Kubota and Nitta*, 2001; *Ohsawa et al.*, 2001; *Hong et al.*, 2006; *Kikuchi and Wang*, 2008]. Because polar-orbiting satellites overpass the same point on the globe only twice a day, their data have been up to now overlooked in favor of infrared observations from geostationary satellites to describe the daily cycle of convection. The latter provide fine-scale, high-temporal resolution information. With the launch of a series of AMSU instruments onboard several platforms the number of overpasses has increased significantly providing an unprecedented opportunity to explore microwave-based data to characterize convective activity in the tropical region; for example, *Hong et al.* [2008] presented a large-scale description of deep convection in the tropical and subtropical regions using seven years of AMSU measurements. Several studies have described the daily cycle of tropical convection showing a contrast between oceanic and continental cycles [e.g., *Kikuchi and Wang*, 2008, and references therein] (hereafter KW08) but they mostly target large areas in the tropics with a general distinction between land and oceanic areas [*Tian et al.*, 2004; *Hong et al.*, 2008]. However, even continental areas present local convective characteristics that may depend on the proximity to the coast, the topography and the land cover [*Durieux et al.*, 2003; KW08].

[4] We focus in this work on the regional aspects of convective activity, specifically on sub-regional scale convection characteristics derived from two sets of different satellites based on microwave emissions, namely, the Advanced Microwave Sounding Unit (AMSU), onboard polar-orbiting NOAA and MetOp platforms, and the 3G68 Land product from the Tropical Rainfall Measuring Mission (TRMM). We compare AMSU and the TRMM 3G68 Land product which is based solely on two microwave instruments, and that constitutes an independent cross-evaluation data set to AMSU. To our best knowledge, such comparisons and more so at regional scale have not been performed before.

[5] We chose an area at the southern edge of the Amazon region, known as the "Arc of Deforestation," which has suffered severe deforestation in the last four decades [*Lepers et al.*, 2005; *Dubreuil et al.*, 2008] with an estimated 15,000 to 25,000 km^2 clearing every year. The state of Mato Grosso, Brazil, is situated within this Arc, and at the very heart of the South American continent (Figure 1). It has suffered intense land cover transformation since the 1970s due to cattle, soybean, corn and cotton farming practices that replaced the original forest and the Brazilian savanna called "cerrado" [*Cardille and Foley*, 2003; *Fearnside*, 2002, 2005; *Morton et al.*, 2006; *Dubreuil et al.*, 2005, 2008, 2012; *Yoshikawa and Sanga-Ngoie*, 2011; *Arvor et al.*, 2012]. Changes in

precipitation and in convective patterns can strongly affect agricultural practices and productivity [*Arvor*, 2009]. The effects of deforestation and atmospheric composition changes (e.g., aeorosols, CO_2) on climate were traditionally addressed in large-scale perspective [*Nobre et al.*, 1991; *Botta and Foley*, 2002; *Oyama and Nobre*, 2003; *Cox et al.*, 2004] while more recent studies have dealt with regional scales [*Durieux et al.*, 2003; *Pongratz et al.*, 2006; *Costa and Pires*, 2010; *Garcia-Carreras and Parker*, 2011]. Observations and numerical models indicate that dry season climate is more affected by deforestation, with lengthening of its temporal extent [*Lee et al.*, 2011; *Wang et al.*, 2011; *Marengo et al.*, 2011]. An extended drought could lead to a northward shift of the "cerrado" [*Nobre et al.*, 1991; *Cox et al.*, 2000, 2004; *Botta and Foley*, 2002; *Oyama and Nobre*, 2003; *Sampaio et al.*, 2007; *Costa and Pires*, 2010] and trigger forest dieback effects [*Cox et al.*, 2004; *Huntingford et al.*, 2008]. However, *Nobre and Borma* [2009] explain that some uncertainty remains as to the effect of heterogeneous patterns of subregional land cover change by increasing precipitation locally through the so-called 'forest breeze' effect [*Roy and Avissar*, 2002; *Ramos da Silva et al.*, 2008; *Garcia-Carreras and Parker*, 2011].

[6] The aim of the present work is thus to describe the temporal characteristics (daily and annual) of the convective regime at regional scale, while comparing convective activity derived from AMSU and TRMM. This will thus allow the evaluation of the impact of land cover and global climate changes at these scales by continuous monitoring and by climate model simulations. Such regional climate models should be able to reproduce the main features of the convective cycle in several temporal and spatial scales. Precipitation climatologies, ground-based rainfall networks and TRMM data have been used for regional climate model validations [e.g., *Correia et al.*, 2008; *da Rocha et al.*, 2009]; the AMSU analysis presented here can be used as an additional source for validation that has been so far overlooked.

[7] The paper is structured as follows: First, data and methods are explained. The subsequent section shows the characteristics of convection in monthly mean time scale and their interannual variability. Section 4 presents an analysis of the diurnal cycle of convection. Possible differences in the convective characteristics over deforested and forested areas are shown in section 5. Finally, the last section contains the discussion and conclusions of the present work.

2. Data and Methods

2.1. Study Area

[8] The target area considered in this study is bounded by 8°–18°S, 50°–63°W and comprises the entire state of Mato Grosso and its immediate surroundings. This region includes a portion of the austral summer rainfall maximum associated with the South American monsoon system, and is also important because it contains the headwaters of the Araguaia and Paraguay rivers which flow into the Amazon and La Plata basins, respectively [*Gan et al.*, 2004]. Figure 1a shows the geographical situation of the target area. We use deforestation data for 2004 provided by the Brazilian National Institute for Space Research (INPE) through the "Program for Deforestation Assessment in the Brazilian
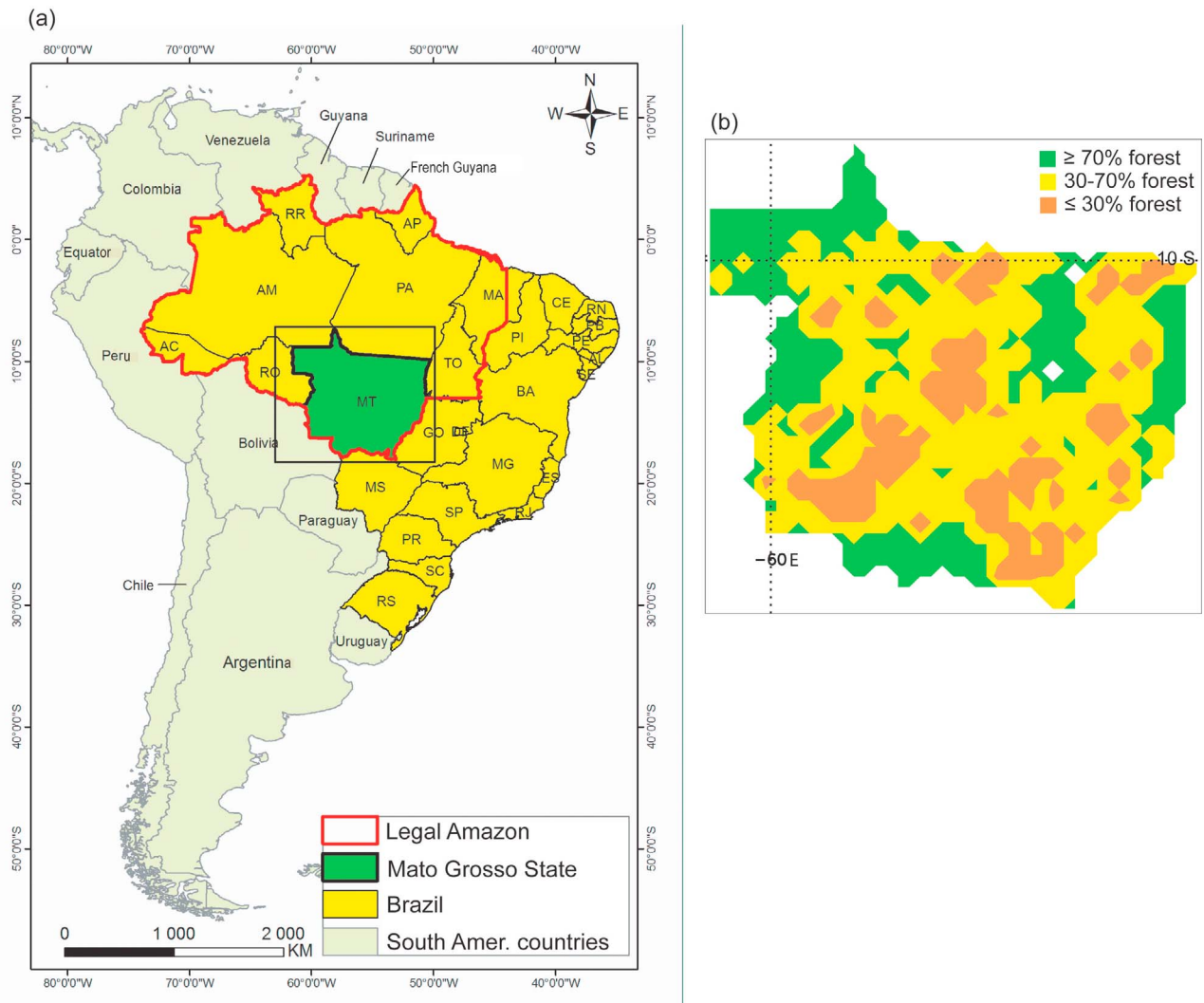
Figure 1. (a) Geographical location of Mato Grosso State (MT; green) within Brazil (yellow) and the South American continent (light green). The red line delineates the area of the so-called "Legal Amazon," and the black box around MT shows the target region considered in the present study. (b) Land cover based on INPE and SEMA-MT deforestation data (see text for details).

Legal Amazonia using remote sensing images and digital image processing techniques" (PRODES project; http://www.obt.inpe.br/eng/prodes.html), and the State Bureau of Environment of Mato Grosso (SEMA-MT). These data, based on images of Landsat and the China-Brazil Earth Resources Satellite, were used to construct a deforestation map with a resolution of 0.25 latitude × 0.25° longitude where percentage of forest is assigned to each grid point (Figure 1b).

2.2. AMSU

[9] AMSU is a cross-scanning, microwave sounder composed of two modules: AMSU-A and AMSU-B. Module A was designed to provide optimal near-surface and atmospheric temperature, and is not used in the present study. Module B has five channels, three of which are centered around 183.3 GHz (channels 3 to 5) and provide information on the atmospheric moisture content from the mid to upper troposphere. While channels 1 and 2 are commonly used for rain retrieval [e.g., *Ferraro et al.*, 2000; *Weng et al.*, 2003; *Lima et al.*, 2007], in the present study we use only data from channels 3 to 5 because they are less affected by the underlying surface [*Deeter and Vivekanandan*, 2005], more sensitive to frozen hydrometeors and therefore useful to detect cold clouds. Module B horizontal resolution is of 16 km at near-nadir and around 48 km at its largest angle; it has a swath width of about 2300 km. We use data from NOAA-15 through 17 AMSU-B, and NOAA-18 and MetOp-A Microwave Humidity Sensor (MHS) data. MHS has very close specifications to the AMSU-B instrument: Channels 3 and 4 have identical frequencies (183.3 ± 1 and 183.3 ± 3 GHz, respectively) in both instruments, while channel 5 is centered at 190 GHz in MHS instead of at 183.3 ± 7 GHz in AMSU-B. The brightness temperature bias between AMSU-B and MHS for channel 5 is estimated to be about 0.1 K, with a standard deviation of 0.1 K [*Kleespies and Watts*, 2006]. Table 1 and Figure 2 show the available satellites carrying AMSU-B or MHS, their launch date and current status.

Table 1. List of Platforms Carrying AMSU Radiometers and Major Characteristics[a]

Platform	Launch Date	LTAN	Operational Status
NOAA-15 (AMSU-B)	13 May 1988	19:20	Channels 3–5 instrument failure since 20 Sep 2010
NOAA-16 (AMSU-B)	21 Sep 2000	14:24	Increased noise in about half track since early 2008 [*Surussavadee and Staelin*, 2010]
NOAA-17 (AMSU-B)	24 Jun 2002	22:25	Channels 3–5 instrument failure since 13 Jan 2010
NOAA-18 (MHS)	20 May 2005	13:41	Normal operation
MetOp-A (MHS)	19 Oct 2006	21:30	Normal operation
NOAA-19 (MHS)	6 Feb 2009	13:43	Channel 3 nominal error exceeding specification of 1 K on 10 Jul 2009

[a]Major characteristics: launch dates, status of AMSU-B/MHS channels 183.3 GHz ± 1, ± 3, and ± 7. LTAN is for Local Time Ascending Node. The value is given at the time of the launching of the satellite. Due to orbital drifts, LTAN in May 2010 is 16:41, 18:25, and 21:04 for NOAA-15, NOAA-16, NOAA-17, respectively. Source: http://www.oso.noaa.gov/poesstatus/ as of January 2011.

[10] We use NOAA-16 and NOAA-18 data covering the periods of July 2001 to June 2005 and July 2005 to June 2011, respectively, to investigate interannual variations of convective activity. We opted for these two platforms instead of NOAA-15 (which has a longer series) because they provide a continuous series with orbital drift of less than one hour in the combined period. NOAA-15 on the other hand has an orbital drift close to 3 h and thus samples different stages of the convective activity throughout the period. NOAA-16 and -18 have very close equatorial crossing hour around 1400 local time (LT) in the ascending node at the selected periods (corresponding to passes over Mato Grosso at around 0200 and 1400 LT) thus ensuring temporally homogeneous 10-year data.

[11] The diurnal cycle of convection was examined for the period July 2002-June 2007, covering five hydrological years. Observations of the diurnal cycle were possible from 2002 onwards, since there were at least three satellites passing over the target region ensuring sampling every four hours on average. In order to preserve the coherence of the diurnal cycle description throughout a given hydrological year, a "new" satellite was added to the computation only in July the next year, for example, NOAA-18 was included in July 2005 and MetOp-A was included in July 2007. Unfortunately data for the period after 2007 was not included as instrumental problems for several NOAA platforms arose that prevented an unbiased handling of the data. Nevertheless we will show that the five years used here provide a robust example of the usefulness of AMSU-B for the depiction of the diurnal cycle of convection in a monthly mean timescale. Hereafter the terms AMSU-B and AMSU will be used interchangeably.

[12] In order to identify convective areas, we use a simple and tractable method, proposed by *Hong et al.* [2005] and based on the three water vapor channels of AMSU-B

(channels 3 to 5). Cold precipitating clouds causes a depression on the AMSU-B channel 3 temperature fields due to scattering of icy particles [*Greenwald and Christopher*, 2002]; channels further away from the center at 183.3 GHz can probe deeper into the cloud, since they are subject to greater scattering from the middle or low layers of the deep convective clouds [*Lima et al.*, 2007]. Based on these properties, *Hong et al.* [2005] defined deep convective areas in the tropical regions as those that satisfy $\Delta T_{17} \geq 0$ K, $\Delta T_{13} \geq 0$ K and $\Delta T_{37} \geq 0$ K (where ΔT_{17} is the difference between the brightness temperatures of channels 183.3 ± 1 and 183.3 ± 7, and similarly for ΔT_{13} and ΔT_{37}). This criterion identifies areas with deep convection (DC) and precipitating clouds, and filters out non-precipitating cold cirrus clouds. *Hong et al.* [2005] showed that their criterion provides a robust screening of strongly precipitating systems in the tropical region; *Funatsu et al.* [2007, 2008, 2009] and *Claud et al.* [2010, 2012] used this criterion for the detection of deep convective areas in the Mediterranean region. Another threshold allows discriminating regions of convective overshooting (COV), that is, $\Delta T_{17} \geq \Delta T_{13} \geq \Delta T_{37} > 0$ K. Convective overshooting refers to clouds which are able to penetrate into the tropopause region and are important in the context of water vapor regulation in the tropical lower stratosphere [e.g., *Holton and Gettelman*, 2001; *Chaboureau et al.*, 2007]. At this point it is important to point out that there is no attempt to determine rain rates, but rather to concentrate on the occurrence of convection, while the intensity is indirectly expressed in terms of area.

[13] Here, for every available pass, AMSU-B/MHS data were re-sampled to a 0.25 latitude × 0.25° longitude grid; only then we computed the relative area of DC and COV to the total satellite pass area. *Hong et al.* [2005] point that the threshold value of 0 K for both DC and COV should be
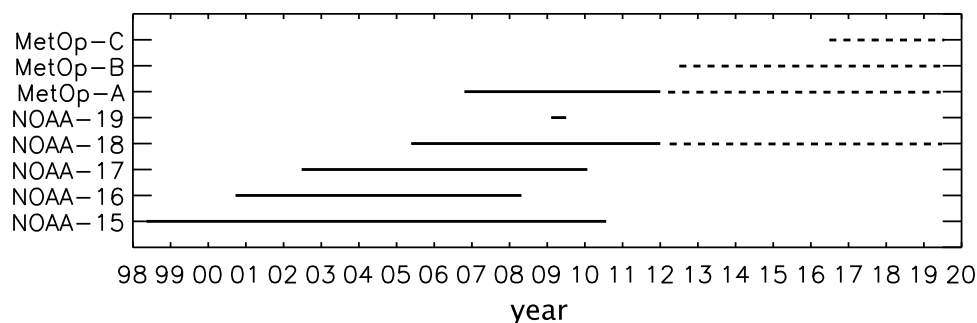
Figure 2. Timeline (as of November 2011) of satellite platforms carrying active AMSU-B (NOAA-15 through -17) or MHS instruments. Dashed lines represent future projections.

(a)   AMSU
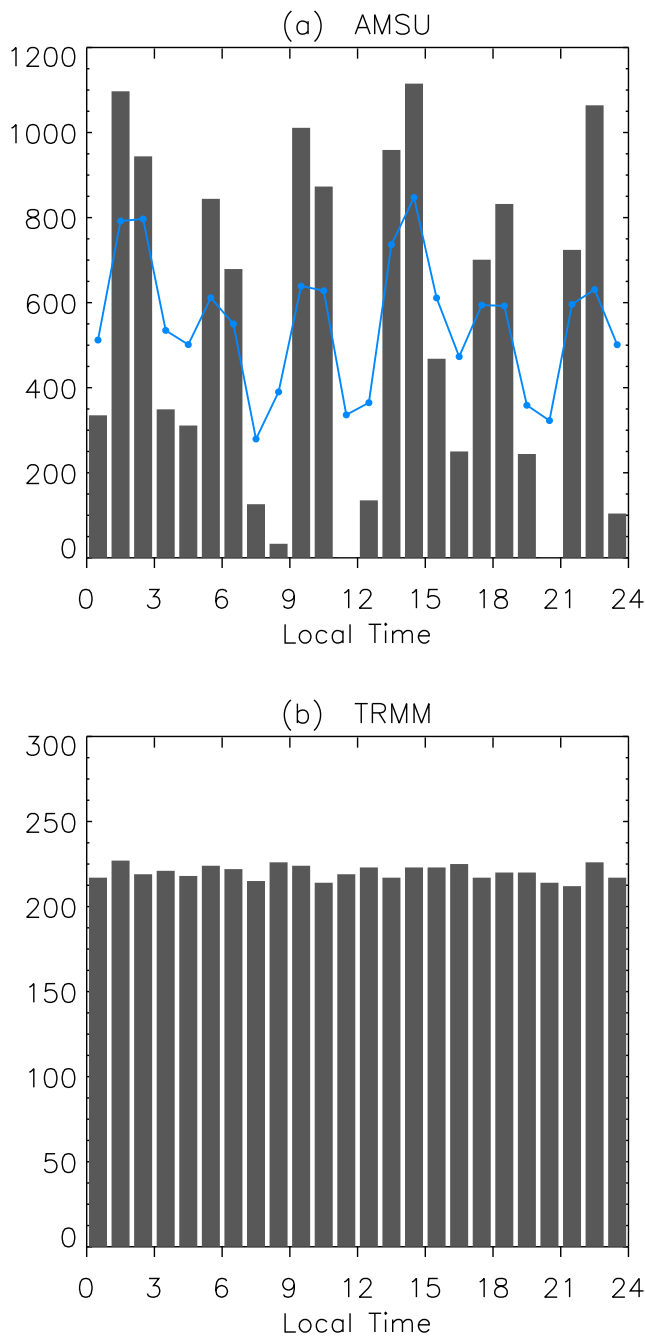
(b)   TRMM

Figure 3. Total number of satellite passes over the target region [18°S, 8°S], [63°W, 50°W] during the period July 2002–June 2007, for (a) NOAA/MetOp and (b) TRMM. For NOAA/MetOp, only passes covering at least 30% of the target area were considered. Note that the y-axes have distinct scales. Blue line in Figure 3a indicates the average number of satellite passes after applying a 3-h running mean for DC and COV calculations.

adjusted for AMSU angle of view (with increased values for larger angles), however because we interpolate AMSU data before calculating ΔTs the angle of view information is lost. This may cause a slight overestimation of DC and COV detection; we will show however that our estimates are of

the same order of those provided by *Hong et al.* [2008] for subtropical land.

[14] Figure 3a shows the number of AMSU-carrying satellite passes considered for each local time, for the period of July 2002 to June 2007. Because NOAA/MetOp satellite passes may not cover the entire area at every pass, only those that cover at least 30% of this area are retained. AMSU has heterogeneous hourly coverage and provides very few or no data between 0700 and 0900 LT, 1100–1200 LT and 2000–2100 LT. Therefore, we calculated the monthly mean DC and COV values at every hour and then calculated a 3-h running mean; this way, the diurnal cycle of convection could be better evaluated. Results of the diurnal cycle analysis based on AMSU will be examined with caution.

2.3. TRMM 3G68 Land Product

[15] TRMM, launched in late 1997, is a joint mission between NASA and the Japan Aerospace Exploration Agency especially conceived for monitoring and studying tropical precipitation [e.g., *Kummerow et al.*, 2000]. After August 2001 the orbit of the satellite was boosted from 350 km to 403 km to extend its lifetime to 2012 [*Cho and Chun*, 2008]. It carries two microwave sensors, namely the TRMM Microwave Imager (TMI) and the Precipitation Radar (PR). TMI is a multichannel passive microwave radiometer that operates at the frequencies of 10.65, 19.35, 37.0, and 85.5 GHz at dual polarization and of 22.235 GHz vertical polarization. The ground resolution varies from 3.5 up to 25 km depending on the radiometer frequency; ground resolution at 85.5 GHz is of 5.1 km. The TMI provides information on the integrated column precipitation content, cloud liquid water, cloud ice, rain intensity, and rainfall types. The PR is the first spaceborne electronically scanning radar, operating at 13.8 GHz horizontal polarization. It provides three-dimensional rainfall distribution over both land and ocean, and defines the layer depth of the precipitation. PR has post-boost ground resolution of 5 km at nadir, but a narrower N-S range of 250 m. The swath width is of 878 km for TMI and 247 km for PR. The TRMM 3G68 Land product integrates information from these two instruments; it provides hourly gridded products based on TRMM 2A12 [*Kummerow et al.*, 2001], 2A25 [*Iguchi et al.*, 2000], and 2B31 [*Haddad et al.*, 1997a, 1997b] rain estimates. Over land, the 2A12 algorithm relies basically on 85 GHz scattering and 37 GHz if scattering/emission signals are available. The 2A12 takes into account mainly deep clouds that have ice particles aloft, while 2A25 senses precipitating size particles, thus retrieving both shallow to deep raining systems. The 2B31 relies on 2A12 estimates adjusted by the 2A25 algorithm over the PR swath, thus combining passive (TMI) and active (PR) microwave measurements. Additional information on the instruments and algorithms can be found at http://rain.atmos.colostate.edu/CRDC/datasets/TRMM_3G68L.html. The TRMM 3G68 product is based solely on TRMM microwave instruments and does not use infrared information (unlike the more widely used TRMM 3B42 product), and thus it arguably provides a more reliable precipitation estimate (KW08). Note however that the TRMM 3G68 is not a standard TRMM product.

[16] Here we use the 3G68 Land combined information of TMI and PR based on the 2B31 algorithm, which accounts
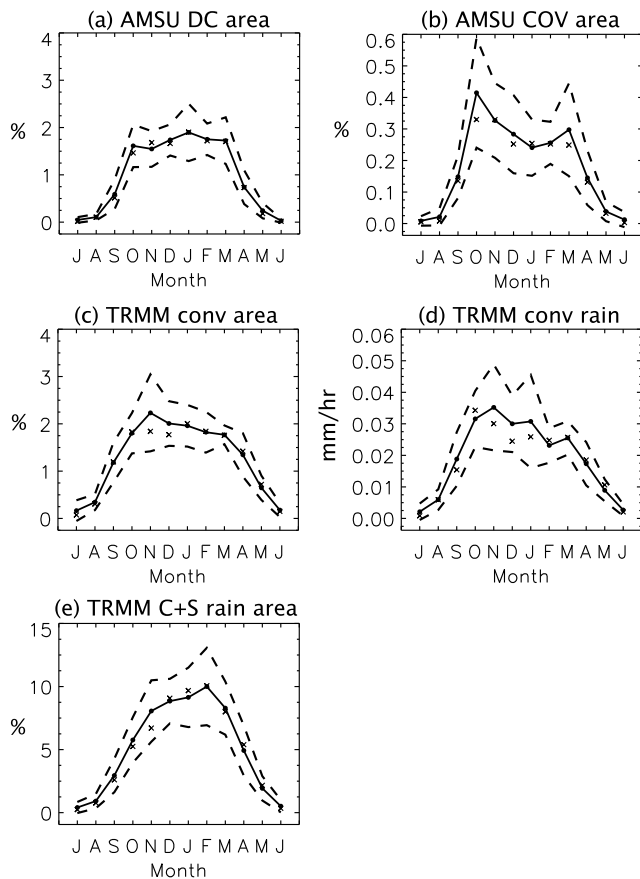
Figure 4. Annual cycle of monthly mean (solid) and median (crosses) convective parameters: (a) AMSU DC area (%), (b) AMSU COV area (%), (c) TRMM convective area (%), (d) TRMM convective precipitation (mm hr^{-1}), and (e) TRMM total (convective and stratiform) rain area (%). Dashed lines indicate the 1-sigma standard deviation. Note that the *x* axis starts in July and finishes in June, following the hydrological year.

for the vertical structure of rainfall (rates and drop-size-distribution parameters) within the PR swath. This product, gridded at 0.1° latitude × 0.1° longitude, contains for each grid point the number of total (nt) and rainy pixels (nr), rainfall estimates (rr), and convective percentage (cp). In order to have quantities comparable to DC and COV from AMSU, we use the convection percentage data to obtain the mean percentage of convective rain pixels ($\sum_{i=1}^{NN}(nr_i* cp_i)/\sum_{i=1}^{NN}(nt_i)$, where NN is the total number of grid points) and mean convective rainfall ($\sum_{i=1}^{NN}(rr_i* cp_i)/\sum_{i=1}^{NN}(nt_i)$). The mean total rainfall area (which includes both convective and stratiform precipitation) is computed as $\sum_{i=1}^{NN}(nr_i)/\sum_{i=1}^{NN}(nt_i)$. Zero rainfall data is included in the calculation of the means.

[17] We use TRMM 3G68 version 6 data available from July 2001 to June 2011, covering one complete decade. All TRMM passes are retained due to its narrower swath width; the high number of passes per day compensates for the limited area sampling at each pass and ensures homogeneous temporal sampling (Figure 3b). TRMM satellite has at least four passes per month at each hour, ensuring 24 h coverage; nevertheless, for the sake of consistency, for the diurnal cycle analysis, a 3-h running mean was also applied to the

computed monthly mean values. Similarly, we used only TRMM data with the same hours of pass corresponding to NOAA-16 and NOAA-18 data for the computation of monthly mean values to investigate interannual variations of convective activity.

3. Multiyear Analysis of Convective Activity

[18] In the central-western region of Brazil, which comprises Mato Grosso and southern Amazon, the rainy season is primarily controlled by the so-called South American monsoon [e.g., *Gan et al.*, 2004]. In this system, the rainy season starts after the period of maximum seasonal temperature [*Gan et al.*, 2004] that acts to destabilize the atmosphere and cause a reversal in the horizontal temperature gradients and vertical wind shear. Typically, the rainy season spans the period of mid-October through mid-March [*Gan et al.*, 2004, 2005; *Carvalho et al.*, 2011]. We examined the annual cycle and time series of monthly evolution of the mean convective activity and its interannual variability based on AMSU and TRMM (Figure 4). First, we notice that the annual cycle is well marked and following the expected climatological minima in (austral) winter and maxima in summer. Furthermore, we note that the values of DC and COV are close to the values estimated by *Hong et al.* [2008] for the Southern Hemisphere subtropical land between 15°–30°S for the period of December 2002 to November 2003 (compare present Figures 4a and 4b with Hong et al.'s Figures 14e and 14f): DC presents a maximum value of nearly 2.0% in January in the present study, and 1.4% in January for their study, and COV maxima of ~0.4% in October in the present study, and 0.4% in February for their study. These differences are small considering the different satellite overpass hours, target areas, as well as the distinct period considered, and they fall within the standard deviation for the nine years considered in the present study.

[19] Figure 4 shows that COV, TRMM convective area and convective rain present a peak early in the beginning of the rainy season (October–November); COV shows a secondary one in March (Figure 4b) but this parameter has the largest standard deviation and thus the mean value is strongly affected by the interannual variability. AMSU DC and TRMM total rainfall have a peak well within the austral summer (January–February). Differences between AMSU DC and COV peaks (in January and October, respectively) might arise because deep convection and convective overshooting have different physical mechanisms of/forcing for development. Unfortunately, such mechanisms cannot be exploited only with the use of diagnostics such as the brightness temperature information from AMSU. Probably a modeling study of cloud formation with detailed microphysics would be necessary to explain such discrepancies, however this is out of the scope of this study. In addition, it is difficult to determine whether the differences in these particular local peaks are important, or an artifact of the relatively short time span, as they could be smoothed out when a longer series will be available.

[20] We then analyzed the time series of each parameter and their anomalies relative to its median seasonal cycle value (Figure 5). The median was preferred because it is a more robust measure than the mean, and allows better emphasizing extreme values in the anomalies. The
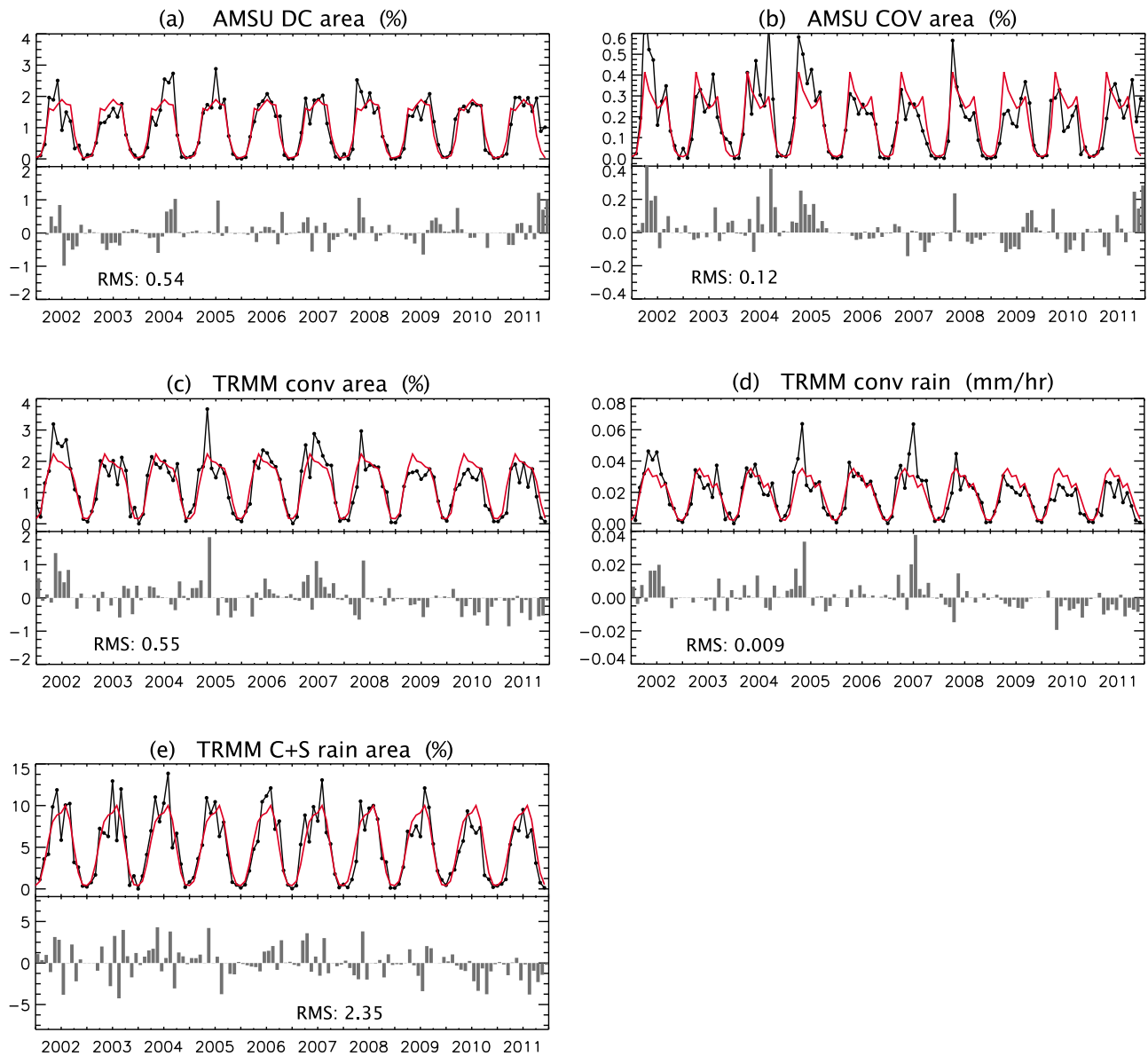
Figure 5. Time series of monthly mean convective parameters (black): (a) AMSU DC area (%), (b) AMSU COV area (%), (c) TRMM convective area (%), (d) TRMM convective rainfall (mm hr^{-1}), and (e) TRMM total rain area (%). Superimposed is the median annual cycle based on the entire period. Bars on the bottom half of each panel denote the anomalies relative to the median cycle, and the root mean square (RMS) of the anomalies is indicated in the lower part.

correlation between the time series of AMSU DC area (Figure 5a) and TRMM convective area (Figure 5c) is 0.77, and AMSU DC and TRMM precipitation (Figure 5d) is 0.69, indicating good agreement between AMSU and TRMM derived quantities. All correlation presented here (and here-after) are significant at least at the 95% level with the Student's t-Test. TRMM convective area and AMSU DC area have a remarkably consistent amplitude estimates, with TRMM showing slightly larger amplitude (about 20%) than that estimated by AMSU. These differences arise partially due to the distinct radiometers, the distinct wavelength emission considered by each instrument, and the methodology to detect convection. Further analysis to explain these differences in amplitudes are presented in the next section.

[21] The time series of the anomalies relative to the median annual cycle, and their RMS values are shown at the bottom half of each panel in Figure 5. The RMS values for AMSU DC and TRMM convective area anomalies are comparable (0.54% and 0.55%, respectively). Normalization of the RMS of the anomalies by the RMS of the original time series shows that the anomalies typically represent 42% and 49% of the total series for respectively AMSU DC and COV, and 36%, 40% and 37% for TRMM convective area, convective rain and total relative rain area, respectively. Even though the anomalies have an overall good agreement in terms of RMS, there is also important interannual variability. In particular, we observe that in the case of COV a spell of several

Table 2. Tendencies of Convective Parameter Anomalies Relative to the Median Value, Based on NOAA-16 and -18 AMSU and TRMM Data, for the Period 2001–2011[a]

	All Months	September and October Only
AMSU DC (%)	0.17 ± 0.11	0.30 ± 0.51
AMSU COV (%)	-0.07 ± 0.03	-0.04 ± 0.11
TRMM conv area (%)	-0.48 ± 0.12	-0.34 ± 0.32
TRMM conv precipitation (mm/hr)	$(-0.09 \pm 0.02) \, 10^{-1}$	$(-0.08 \pm 0.06) \, 10^{-1}$
TRMM total rain area (%)	-1.53 ± 0.54	-2.49 ± 2.00

[a]Values are given in decade^{-1}, with 1-sigma uncertainty level.

anomalously low values is seen from 2006 to early 2011 (Figure 5b), while for TRMM parameters negative anomalies are predominant after 2008 (Figures 5c–5e).

[22] It is tempting to look at tendencies of these parameters even if the short time span prevents calculation of significant, long-term trends. For the sake of the exercise, we derived the linear tendencies for the convective parameters based on the time series of anomalies relative to the median seasonal cycle. The term "tendency" is used here since the short time span prevents strict trend calculations. Except for AMSU DC, all parameters show a slight negative tendency (see Table 2) when considering all months in the period. The largest decrease is given by TRMM convective area, which presents a tendency of -0.48 ± 0.12%/decade, whereas AMSU DC tendency presents a positive value of 0.17 ± 0.11%/decade. The latter seems to be strongly influenced by the large positive anomaly seen in the end of the period (end of rainy season in 2011), which is not reproduced by TRMM. TRMM convective area negative tendency is much stronger than that estimated for AMSU DC by *Hong et al.* [2008] for the entire tropical belt, of -0.016%/decade, based on NOAA-15 AMSU from 1999 to 2005. AMSU COV presents a negative tendency of -0.07 ± 0.03%/decade which is comparable with the value of -0.142%/decade found by *Hong et al.* [2008]. These differences could be due not only to the differences in period, but also on the regional aspect of the present analysis which encompasses the issue of the specific land use (as opposed to an average of the whole tropical region). TRMM-derived tendencies for convective precipitation and total are also negative, with values of $-0.09 \pm 0.02 \; 10^{-1}$ (mm.hr^{-1})/decade and -1.5 ± 0.5%/decade), respectively. *Fu and Li* [2004] suggest that if changes in land use in the Amazon reduce rainfall during dry and transition seasons, it could significantly delay the onset of the wet season.

[23] We also calculated tendencies for the combined months of September and October only (Table 2), when the transition from dry to rainy season takes place. It is usually in the second half of October that seeds are planted, and rainfall is expected within about 2 weeks, after which the seed is lost. Again, all convective parameter tendencies except for AMSU DC are negative, that is, suggestive of a shift to drier conditions (e.g., -0.34 ± 0.32%/decade for TRMM percentage of convective pixels, $-0.08 \pm 0.06 \; 10^{-1}$ (mm.hr^{-1})/decade for convective precipitation, and -2.5 ± 2.0%/decade for total rainfall area). These values have large uncertainties due to the short period and may not be evaluated as a real trend, yet they suggest a tendency in recent years for a delay in the

beginning of the rainy season. Although *Carvalho et al.* [2011] have not found any changes in the period of onset of the rainy season for the whole of the Amazon basin, the present result is resonant with the work of *Butt et al.* [2011] who found a shift of an average of 11 days for the beginning of the rainy season in regional scale, focusing on a heavy deforested region in western Amazon.
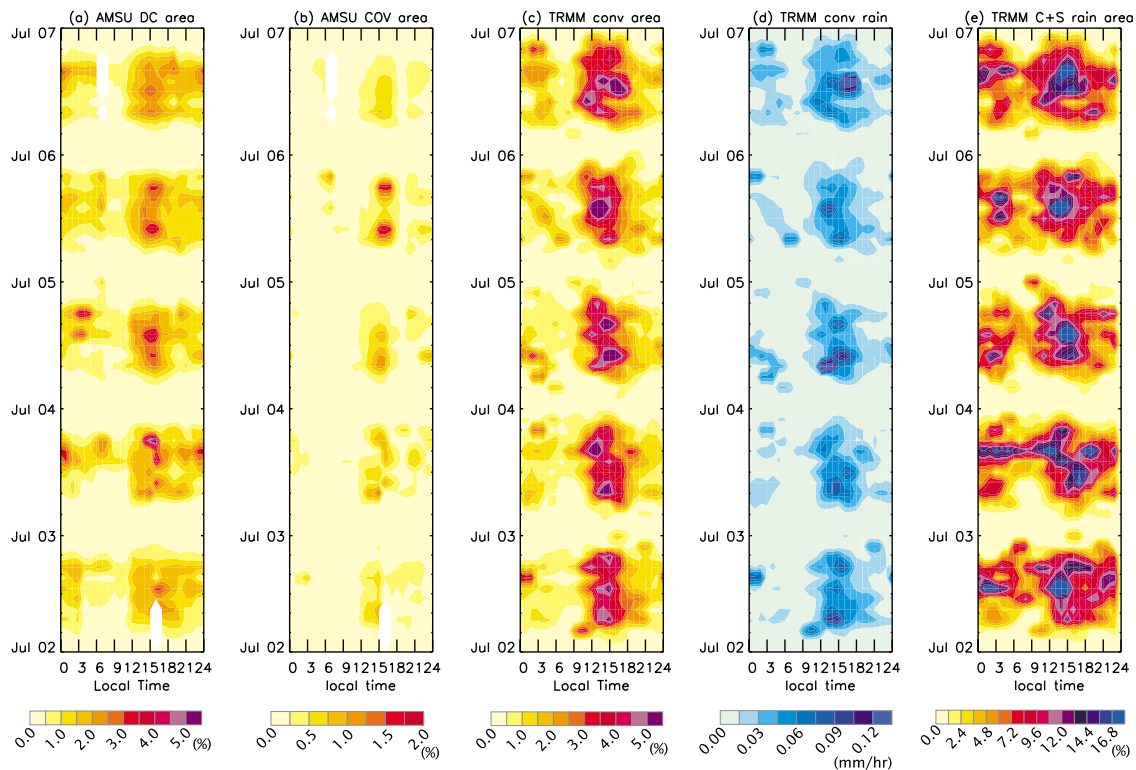
4. Diurnal Cycle of Convection

[24] In a first step we examined whether the derived description of the diurnal cycle is realistic by comparing the annual mean DC area with rain gauge data at the station of Alta Floresta (9°53′S, 56°5′W [*Dubreuil et al.*, 2012]), for the hydrological year 2006/2007 (Figure 6). The diurnal cycle of precipitation at Alta Floresta and the evolution of convection observed by satellites have a fairly good agreement. The development of convection and precipitation starts after 1100 LT. All data sets show maximum convective area (AMSU and TRMM) or precipitation (rain gauges) between 1500 and 1600 LT, and minima between 0800 and 0900 LT. The correlation between AMSU and rain gauge is of 0.82, while that between TRMM convective area and rain gauge is of 0.76. Since these data are completely independent, it supports at least qualitatively the description of the diurnal cycle of convection not only from TRMM, but also from AMSU/MHS which had not been shown before.

[25] The monthly mean diurnal cycle of convection for the period July 2002 to July 2007 is presented in Figure 7. There is a fast increase in the convective activity around noon in October corresponding to the beginning of the wet season. AMSU DC is largest around 1500 local time (LT). AMSU DC area increases until January and then decreases substantially after February (Figure 7a). As the rainy season advances DC extends throughout the night showing a secondary maximum around 0000 to 00400 LT from January to April.
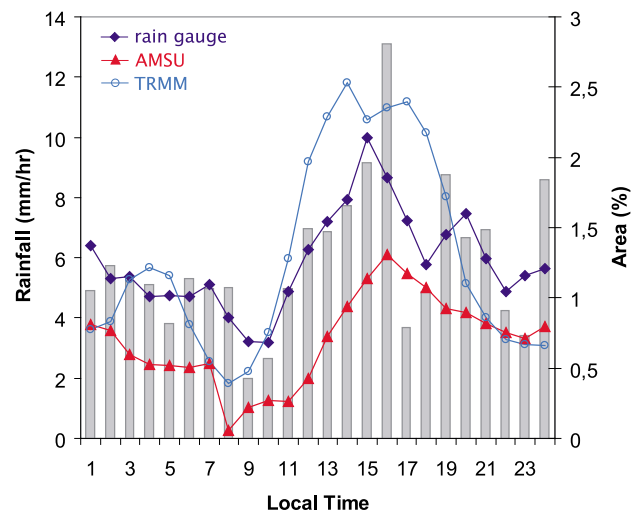
Figure 6. Average hourly distribution of rainfall (gray bars, mm hr^{-1}) based on the period August 2006–August 2007 at the station of Alta Floresta, Mato Grosso. Superimposed are the 3-h running mean of rainfall (dark blue, mm hr^{-1}), AMSU DC (red, %) and TRMM 3G68 (light blue, %) convective areas.

Figure 7. Monthly mean diurnal cycle of the relative area of (a) AMSU DC (%), (b) AMSU COV (%), (c) TRMM convective area (%), (d) TRMM mean convective rainfall (mm hr^{-1}), and (e) TRMM total rain area (%). The abscissa indicates the local time.

The end of the wet season (March–April) is marked by a rather sudden decrease in DC area. The COV area represented between 20 to 40% of the DC area (Figure 7b), in good agreement with the results of *Hong et al.* [2005] who estimated the ratio COV/DC in 26% for the whole of the tropical belt based on the period of March 2003 to February 2004. This ratio presents large day to day variability (not shown) and can reach 100% in a daily mean basis, that is, it is possible in a certain day to have exclusively COV. It attains a maximum at around 1500 LT or later during the rainy season.

[26] The analysis of TRMM data reveals similar features of those from AMSU, as seen by the temporal evolution of percentage of convective rain pixels, mean convective rainfall and mean total rainfall area (Figures 7c–7e). All parameters show maxima between 1200 and 1700 LT, close to that found from AMSU analysis. After this period most of the convective clouds are replaced by middle level clouds (Figure 7e): While the maximum values of convective area are found mostly during the afternoon (with few elements of convective clouds active during the night), comparable values of large total rain area are found both in the afternoon and between 00 and 03 LT. It is thus reasonable to infer that these larger values during nighttime are either from anvils from dissipating deep convective clouds, or from mid- to low level clouds since the signal of convective area decreases at the same hours. Mesoscale convective complexes, which are ubiquitous features in the extended summer season in South America, may contribute to convective activity at nighttime in this region [e.g., *Durkee and Mote*, 2010] however because they are extremely long-lived (average duration of

14 h) they do not correspond to the diurnal cycle observed here.

[27] Both data sets also show intraseasonal variability [*Ferreira and Gan*, 2011] with active periods and some breaks within the rainy season. As the rainy season advances, convection generally appears slightly earlier in the day (e.g., Figure 7c, 2003/2004). The relative area of convective rain pixels estimated by TRMM is however larger than that estimated by AMSU using *Hong et al.* [2005] DC threshold, roughly by 50%. A slight difference in the convection description is found between AMSU and TRMM (e.g., Figures 7a and 7c): AMSU shows a period of relative decreased convective activity between January–March 2006, whereas during this period TRMM shows maximum percentage of convective pixels and convective precipitation. Since these differences appear at a time of the day that is well covered by AMSU, temporal sampling alone cannot explain such discrepancies. They are likely a combination of a slight difference in the hours of satellite overpass, the distinct diagnostics for detection of convection (AMSU essentially captures deep convective clouds with anvils while TRMM algorithms include empirical distributions of droplet sizes to distinguish convective and stratiform precipitation), and distinct spatial sampling as TRMM microwave instruments have a narrower swath width than that of AMSU.

[28] To further investigate the impact of distinct AMSU DC and TRMM convection detection methodologies on the estimation of convective areas, we analyzed the upper tropospheric humidity (UTH) distributions when (i) AMSU DC was found, and (ii) TRMM convective percentage ≥80% was
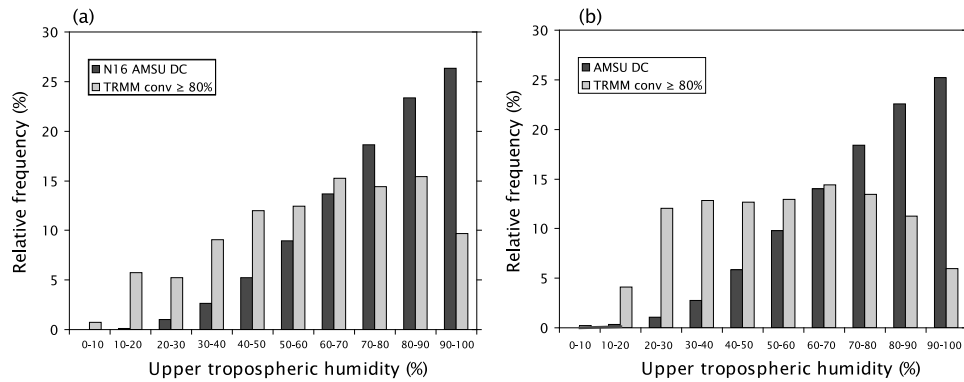
Figure 8. Upper tropospheric humidity (UTH) distributions for cases when AMSU DC (dark gray) or TRMM convective percentage >80% (light gray) were found. UTH is relative to ice; only UTH ≤ 100% were considered. The period considered was October 2002 to April 2003. (a) Distribution using only NOAA-16 satellite data, which overpasses the target region around 0200 and 1400 LT, and (b) distribution using NOAA-15, -16 and -17, covering several hours of the diurnal cycle.

found. We used AMSU channel 3 data to obtain UTH following *Buehler and John* [2005]. Such UTH is representative of a relatively broad atmospheric layer centered at around 6–8 km, and gives indication on the saturation relative to either water or ice content. Here we calculated the saturation relative to ice because we are interested in cold clouds; although supersaturation can occur, only UTH ≤ 100% were considered. We used TRMM passes within ±10 min of the NOAA satellite pass hour over the state of Mato Grosso, and considered TRMM pixels that fell within ∼30 m of the AMSU grid point. The period considered for this analysis was Oct 2002–Apr 2003.

[29] Figure 8a shows the UTH distribution based only on NOAA-16 satellite data, which overpasses the target region at around 1400 LT, thus sampling the hour that we found is close to the maximum convective activity, while Figure 8b shows the UTH distribution using NOAA-15, -16 and -17, covering several hours within the diurnal cycle. Both histograms indicate that in about 50% of the cases when AMSU DC is found UTH is larger than 80%, whereas for TRMM, UTH has a more spread distribution including lower UTH values. This indicates that TRMM includes shallower convective clouds (which do not saturate with respect to ice at the upper troposphere). This result helps explain the apparent discrepancies in the amplitude and duration of convective activity depicted by AMSU and TRMM in Figure 7. In the case where we consider the hours closer to
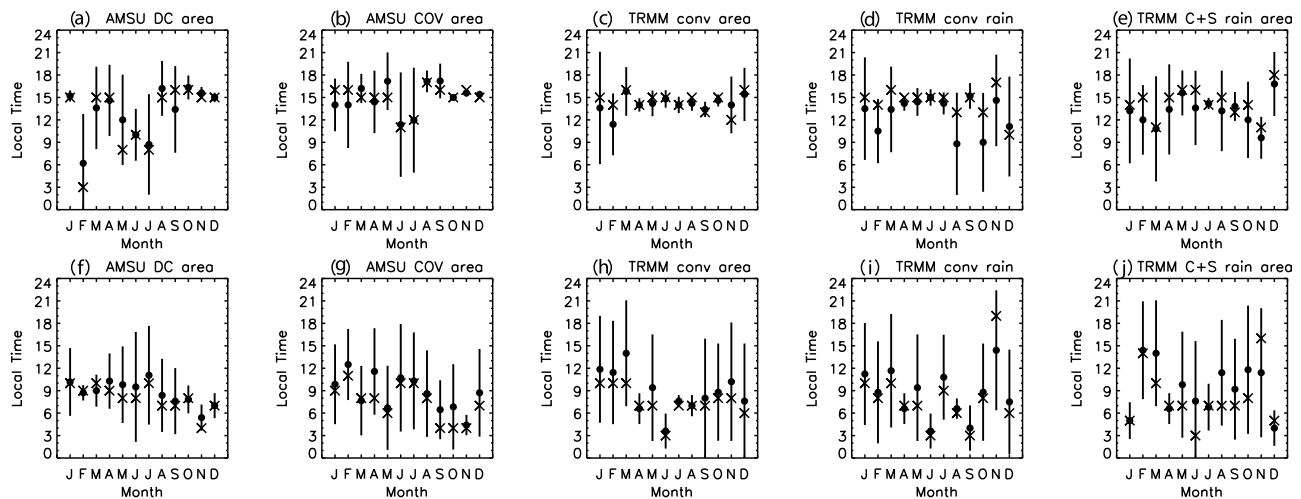
the maximum convective activity (Figure 8a) UTH distributions for TRMM are more skewed toward saturation compared to the situation where the entire diurnal cycle is considered (Figure 8b), when the distribution is more spread. Finally, this result further clarifies why the differences in the amplitudes of convective areas by TRMM and AMSU found in the previous section are smaller than those found here.

[30] Figures 9 and 10 present the frequency distribution and the month to month variability, respectively, of the hours of peak and minimum activity for AMSU-derived DC and COV areas, and TRMM-derived percentage of convective pixels, convective rainfall and total rainfall area. There is a good agreement between the different parameters and instruments, despite the satellites distinct temporal coverage. Maximum convective activity is found in the afternoon between 1500 and 1600 LT while the minimum hour of convective activity is mainly concentrated between 0600 and 1000 LT (Figure 9). The time window for the minimum activity coincides with a substantial decrease in AMSU coverage; however TRMM results support the finding of minimum activity in early morning. These results are consistent with those by KW08, who found that convection over land only (all continental areas between 40°N-40°S) is predominantly concentrated between 1200 and 1800 local solar time, with a minimum around 0600 local solar time.

[31] The month to month variability in the hours of maximum convective activity shows a remarkable consistency in
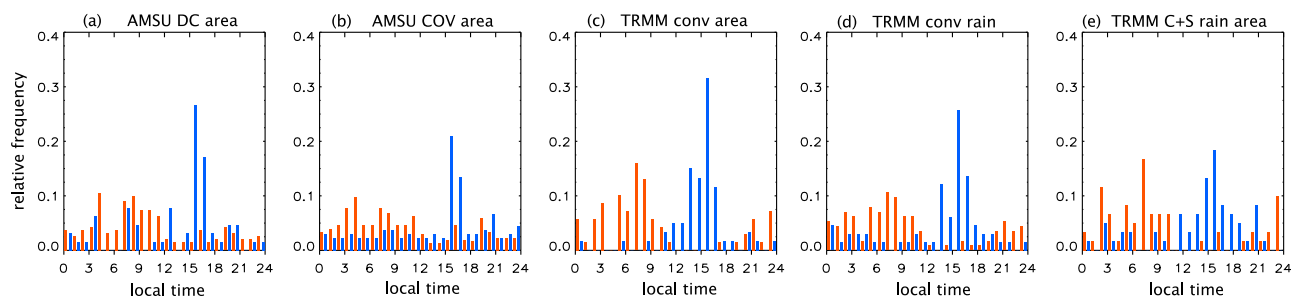
Figure 9. Relative frequency of hours of maximum (blue) and minimum (orange) convective activity from AMSU-derived (a) DC and (b) COV areas, and TRMM-derived (c) percentage of convective pixels, (d) convective rainfall, and (e) total rain area.

Figure 10. Interannual variability of the hour of (a–e) maximum and (f–j) minimum convective activity and total precipitation. Mean value is marked as a circle, median as an x, and bars denote the standard deviation.

the hour of maximum for all months, around 1500 LT. There is however large variability particularly between February and August for AMSU DC (Figure 10a), and in June and July for AMSU COV (Figure 10b). The large variability depicted by AMSU in the hours of maximum convection in the austral winter in this region may be partially explained by convective forcing by synoptic (frontal) systems originated from the south, which can account for up to 50% of the daily convective variability [*Siqueira and Machado*, 2004]. This winter variability in the hour of maximum convection occurrence is not captured by TRMM, which shows larger variability in the rainy season, and reduced variability in the dry (winter) season. The maximum DC and COV compared to their mean values in winter are as small as for TRMM parameters (not shown), indicating that the large variability in the hours of maximum convection for AMSU in the austral winter are meaningful. The minimum hours for all convective parameters (Figures 10f–10j) show a larger scatter of the mean and larger variability than the maximum.

5. Forested Versus Deforested Convective Activity

[32] We repeated the above analysis separating deforested and forested areas. We considered "forested" areas as those with at least 70% of forest, while "deforested" were those with less than 30% of forest (Figure 1b). The convective activity over forested and deforested areas do not show significant differences in the phase of diurnal cycle, however TRMM and AMSU depict a somewhat distinct pattern of convective characteristics over these two surfaces. Both data sets indicate that deforested areas have a larger maxima of convective activity in monthly mean basis particularly in the beginning of the rainy season, in October–November (Figure 11), in agreement with earlier observational studies that found enhanced rainfall with increased deforestation in timescales of months [*Silva Dias et al.*, 2002] to years [*Durieux et al.*, 2003]; the month of December seems to be an exception with TRMM parameters showing a reverse behavior. We tested whether the monthly mean differences between the convective parameters for forested and

deforested areas are significantly different using the t-Test, i.e., we tested whether the difference of the two sample means is significantly different from zero. We found that for AMSU DC and TRMM convective area these differences are significant at ~98% while for COV the significance is lower, ~90%. For TRMM convective rain and total rain area, the significance drops to less than 80%. Overall, these statistical tests demonstrate that, although small, the differences between convective parameters over deforested and forested areas are significant. The RMS analysis for each series (deforested and forested) point to slightly larger values of convective activity over deforested than forested areas (Table 3), but differences in convective precipitation are very small.

[33] While the average behavior given by TRMM and AMSU is roughly similar, individual years may present important differences (Figure 12). For example, AMSU shows larger DC areas over deforested areas in 2005 (which was a drought year) and 2007 (Figures 12a and 12b), while TRMM shows the opposite (Figures 12c–12e). Conversely, TRMM data shows more convection (Figures 12c and 12d) and overall precipitation (Figure 12e) over forested areas in 2006, which is not well captured by AMSU (Figures 12a and 12b). The RMS of the differences in convective activity (RMSd) between deforested and forested areas are shown in Table 3. The RMSd of AMSU DC is smaller than that of TRMM convective area (0.50% and 0.83%, respectively), but normalization with respect to the RMS of the "deforested" series indicate that these anomalies have closer values, 34% and 42%, respectively. AMSU COV and TRMM convective rain have relatively large RMSd when compared to RMS of either "forested" or "deforested" series. Tendencies based on the difference between deforested and forested areas indicate that all convective parameters except for AMSU COV lean toward increased (decreased) precipitation in deforested (forested) areas, for example, $+0.08 \pm 0.16$%/decade for AMSU DC, and $+0.25 \pm 0.28$%/decade for TRMM convective area. The total rain area shows a decreasing trend, -0.38 ± 0.73%/decade. Because of the short time series, these results must be taken with caution. An extensive discussion on the
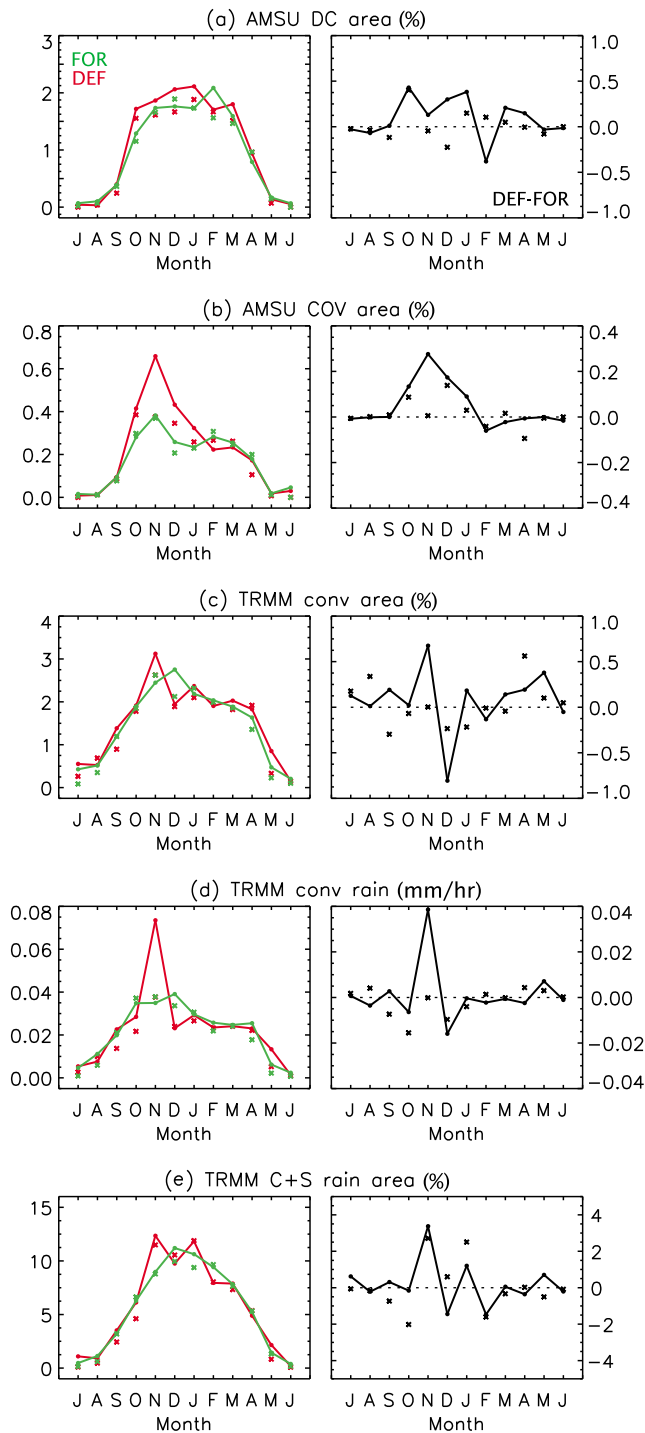
Figure 11. (left) Annual cycle (starting in July) of monthly mean (solid) and median (crosses) convective parameters for deforested (red) and forested (green) areas (see Figure 1b); (right) difference between deforested and forested monthly mean and median values. (a) AMSU DC area (%), (b) AMSU COV area (%), (c) TRMM convective area (%), (d) TRMM convective precipitation (mm hr^{-1}), and (e) TRMM total relative area of rain (%). The x axis starts in July and finishes in June, following the hydrological year.

Table 3. Root Mean Square Values of Convective Parameters for Deforested (DEF), Forested (FOR), and Difference Between Deforested and Forested Areas

	DEF	FOR	DEF-FOR
AMSU DC (%)	1.48	1.31	0.50
AMSU COV (%)	0.36	0.22	0.22
TRMM conv area (%)	2.00	1.73	0.83
TRMM conv precipitation (mm/hr)	0.04	0.03	0.03
TRMM total rain area (%)	7.25	7.01	2.26

implications and caveats of the present analysis is included in the next Section.

6. Summary and Discussion

[34] This study presented a description of the convective regime characteristics in regional scale, for the state of Mato Grosso, Brazil, which has been severely deforested in the last four decades. Our study is based solely on microwave observations from AMSU and TRMM. The present results are novel since we target a very restricted domain using data from polar-orbiting satellites, which have not been extensively used for monitoring diurnal cycle mainly due to temporal sampling issues. Deep convection and convective overshooting from the AMSU instrument are derived from a criterion proposed by *Hong et al.* [2005], which is very attractive due to its simplicity and because it is rather insensitive to the ground influence. Moreover, since it is based on differences of channels, possible inter-satellite biases are reduced. TRMM 3G68 2B31 is a combined passive-active microwave data product which yields a better temporal representation of precipitation patterns than estimates derived from infrared data (KW08). Here we use data in the period of July 2001 to June 2011, covering one complete decade.

[35] The time series of mean convective activity and monthly mean anomalies, as well as the seasonal cycle show that the interannual variability can be rather large. Based on this 10-year period we found that all convective parameters except AMSU DC show negative tendencies (i.e., decrease in convective activity), which is also noted when isolating the months of September and October (transition from dry to rainy season). The decadal tendency estimated here must be interpreted with caution, because the data sets are different, the time series are short and the estimation of tendencies may be sensitive to the initial/end values. Nevertheless, the results presented have possible implications for agricultural practices as the level of agricultural intensification, such as the adoption of double cropping systems, is strongly dependent on the length of the rainy season [*Arvor*, 2009]. This negative shift is seemingly in conflict with the trends observed by e.g., *Marengo* [2004] that used multidecadal (1929–1999) rain gauge and gridded products to study long-term rainfall variability in the whole of the Amazon basin. *Marengo* [2004] found that the Southern part of the Amazon basin indicate a positive rainfall anomaly (depending on the data set used) more in line with observed rainfall changes in Southern Brazil, which was explained as related to increased activity of extratropical perturbations typical of El Niño years. However, that study domain includes a region much larger than that used here and a different period. Besides, here we look specifically at convective activity characteristics, which are affected by the
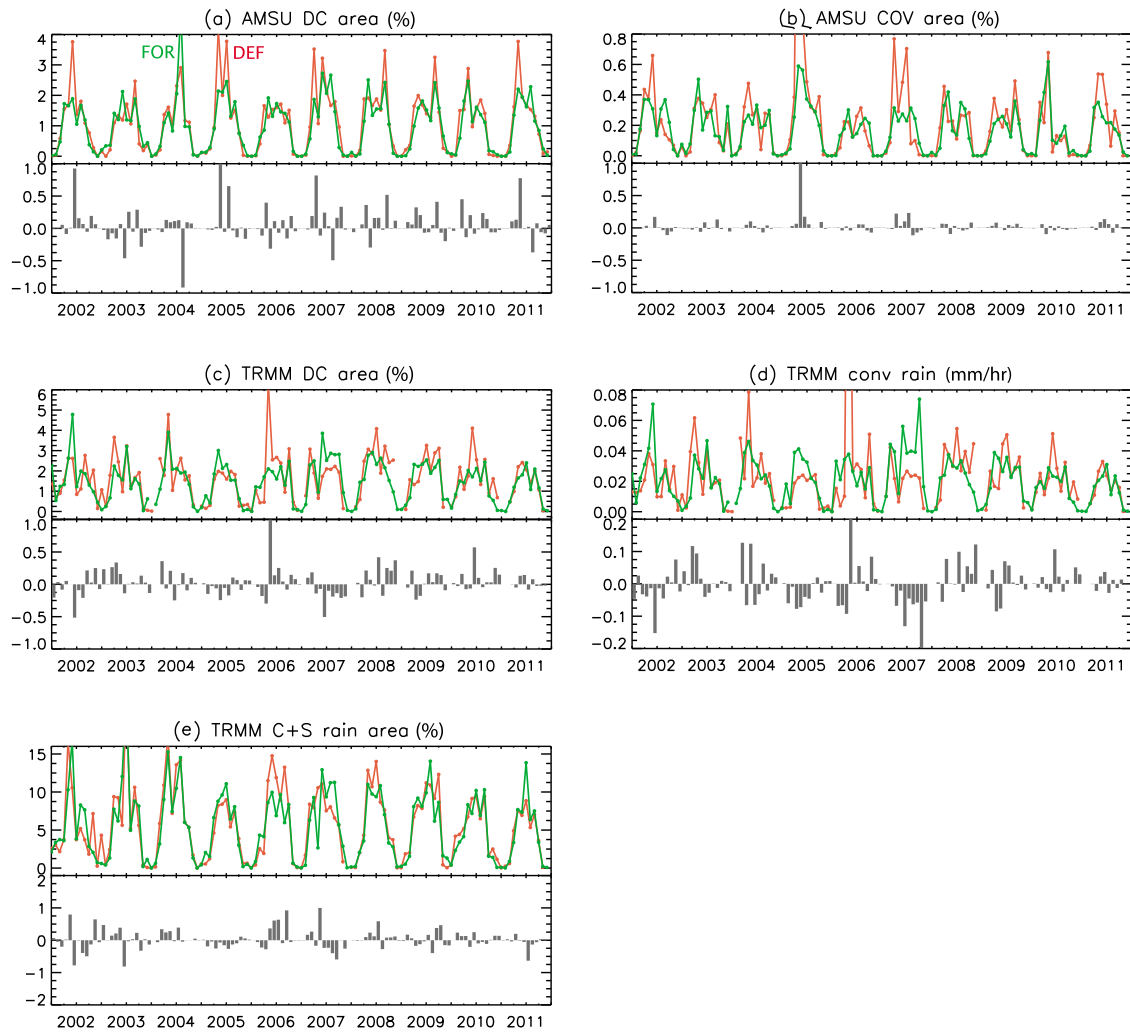
Figure 12. Time series of monthly mean convective parameters for forested (green) and deforested (red) areas (as in Figure 1b): (a) AMSU DC area (%), (b) AMSU COV area (%), (c) TRMM convective area (%), (d) TRMM convective rainfall (mm hr^{-1}), and (e) TRMM total relative rain area (%). Bars on the bottom half of each panel denote the difference values between deforested and forested areas, normalized by the largest absolute difference value in the period.

increased aerosol loading due to biomass burning that may have an impact on convection occurrence and timing.

[36] In terms of the diurnal cycle of convection, we found that its description based on as many as three polar-orbiting satellites can be rather satisfactory, provided that overpasses are more or less evenly spaced in time. The analysis based on 5-yr (2002–2007) AMSU and TRMM data showed that deep convection over the state of Mato Grosso is mostly concentrated in the afternoon, with maximum activity around 1500 LT, but can also be found during nighttime. Minimum convective activity is usually found in the early morning, between 0700 and 0900 LT. AMSU passes present a window without overpasses exactly at this period, but analysis of TRMM data corroborates this result. The hour of peak activity is in close agreement with the temporal phase derived by KW08 based on the first component of the principal component analysis (PCA) of 9-years of TRMM 3G68 data (1998–2006) for the tropical region; however the minimum hour is slightly off (their minimum was found at around 0600 LT). Estimates of the diurnal cycle over land based on

infrared satellite data often show convection peak later in the day, around 1800 LT (KW08) or even 2000–2400 LT [*Tian et al.*, 2004]. These estimates are usually made based on large areas, while here we focus on a relatively small area and therefore our results provide a more reliable representation of a specific region. The temporal phase of the diurnal cycle shows little variation with season, despite amplitude differences. The largest variability found with AMSU data was during the dry season, with important variability contribution due to synoptic systems advancing from the south [*Siqueira and Machado*, 2004].

[37] Differences between convective activity over deforested and forested areas point to a slight larger value over the former. There is also indication of an increase (decrease) of precipitation over deforested (forested) areas particularly in the beginning of the rainy season, however uncertainties are large. A caveat of our analysis is that it was based on land use data of 2004, when there was the largest deforestation rate in Mato Grosso state in the decade. Therefore, areas that were assigned as deforested could well have been forested

between 2002 and 2004 thus introducing a bias. In addition, the land cover classification used here (i) does not discriminate forests, cerrado and Pantanal in the "forested areas," and (ii) does not differentiate pasture, crop or secondary forest in "deforested areas." Mato Grosso state has a very heterogeneous land cover, and this heterogeneity implies distinct heat and humidity fluxes partitions [*Fu and Li*, 2004; *Roy and Avissar*, 2002], which were not studied here. In general, observations of climate change over large deforested areas find increase of surface temperature and decrease in evapotranspiration [*Pielke*, 2001; *von Randow et al.*, 2004], however changes in precipitation are more difficult to detect [*Nobre and Borma*, 2009], and long time series are necessary to obtain reliable statistics.

[38] In light of the above caveats, results of section 5 should be considered with caution, under the context of spatial scale and the degree of deforestation. Previous numerical simulation studies have shown that deforestation in scales of tens to up to some hundreds of km^2 can lead to a "vegetation breeze effect" resulting in a local increase in precipitation in deforested areas [*Avissar and Schmidt*, 1998; *Davidson et al.*, 2012]. Furthermore, partial or heterogeneous deforestation can buffer against potential climate-tipping points and protect the drier ecosystems of the basin by leading locally to an initial increase in precipitation [*Correia et al.*, 2008; *Walker et al.*, 2009]. However, after a certain deforestation level this condition would become unsustainable, resulting in drier conditions and reduced precipitation in the region. Finally, changes in temperature and precipitation depend also on the subsequent land use type [*Sampaio et al.*, 2007; *Costa et al.*, 2007]. For instance, the substitution of forest by either soybean agriculture or pasture under a business-as-usual scenario would lead to consistent decrease in rainfall, the decrease stronger with soybean land cover. All these issues should be considered for a complete assessment of the long-term deforestation effects on climate.

[39] Overall, AMSU and TRMM 3G68 2B31 provide a congruent depiction of the convective activity at regional to local scale, here specifically for the state of Mato Grosso. Differences in the convective characterization by AMSU DC and TRMM arise from the fact that unlike AMSU DC criteria, which detects deep convective clouds with very cold, saturated tops, TRMM considers both relatively shallow and deep convective clouds. It would be interesting as well to perform comparisons of AMSU and other TRMM products based solely on the PR (such as the 2A25 or 3A25 products), as this instrument is specially designed to give a three-dimensional description of rainfall and could give additional information on the height of the storms and on the ability of AMSU to capture different stages of convective lifecycles. Despite the failure of AMSU-B/MHS in some NOAA platforms, the upcoming launch of two MHS-carrying Metop satellites in 2012 and 2016 (Figure 2) will contribute to the continuity of the AMSU data. The present work highlights the usefulness of microwave observation as a valuable source for monitoring and estimating convective activity patterns at regional scales, and offers an additional source for model verification. An example of the usefulness of such analysis on the evaluation of climate model uncertainties for the Mediterranean region was recently demonstrated by *Claud et al.* [2012]. This type of comparisons could be similarly applied for regional modeling evaluation in other regions,

including climate simulations of the impact of heterogeneous deforestation in the Amazon basin.

References

Aceituno, P. (1988), On the functioning of the Southern Oscillation in the South American sector. Part I: Surface climate, *Mon. Weather Rev.*, *116*, 505–524, doi:10.1175/1520-0493(1988)116<0505:OTFOTS>2.0.CO;2.

Arkin, P. A., and B. N. Meisner (1987), The relationship between large-scale convective rainfall and cold cloud cover over the western hemisphere during 1982–1984, *Mon. Weather Rev.*, *115*, 51–74, doi:10.1175/1520-0493(1987)115<0051:TRBLSC>2.0.CO;2.

Arvor, D. (2009), Etude par teledetection de la dynamique du soja et de l'impact des precipitations sur les productions au Mato Grosso (Bresil), PhD thesis, 396 pp., Univ. Rennes 2, Rennes, France. [Available at http://tel.archives-ouvertes.fr/tel-00422109.]

Arvor, D., M. Meirelles, V. Dubreuil, A. Begué, and Y. E. Shimabukuro (2012), Analyzing the agricultural transition in Mato Grosso, Brazil, using satellite-derived indices, *Appl. Geogr.*, *32*, 702–713, doi:10.1016/j.apgeog.2011.08.007.

Avissar, R., and T. Schmidt (1998), An evaluation of the scale at which ground-surface heat flux patchiness affects the convective boundary layer using a large-eddy simulation model, *J. Atmos. Sci.*, *55*, 2666–2689, doi:10.1175/1520-0469(1998)055<2666:AEOTSA>2.0.CO;2.

Botta, A., and J. A. Foley (2002), Effects of climate variability and disturbances on the Amazonian terrestrial ecosystems dynamics, *Global Biogeochem. Cycles*, *16*(4), 1070, doi:10.1029/2000GB001338.

Buehler, S. A., and V. O. John (2005), A simple method to relate microwave radiances to upper tropospheric humidity, *J. Geophys. Res.*, *110*, D02110, doi:10.1029/2004JD005111.

Butt, N., P. A. de Oliveira, and M. H. Costa (2011), Evidence that deforestation affects the onset of the rainy season in Rondonia, Brazil, *J. Geophys. Res.*, *116*, D11120, doi:10.1029/2010JD015174.

Cardille, J., and J. A. Foley (2003), Agricultural land-use change in Brazilian Amazonia between 1980 and 1995: Evidence from integrated satellite and census data, *Remote Sens. Environ.*, *87*, 551–562.

Carvalho, L. M. V., C. Jones, A. E. Silva, B. Liebmann, and P. L. Silva Dias (2011), The South American monsoon system and the 1970s climate transition, *Int. J. Climatol.*, *31*, 1248–1256, doi:10.1002/joc.2147.

Chaboureau, J. P., J.-P. Cammas, J. Duron, P. J. Mascart, N. M. Sitnikov, and H.-J. Voessing (2007), A numerical study of tropical cross-tropopause transport by convective overshoots, *Atmos. Chem. Phys.*, *7*, 1731–1740, doi:10.5194/acp-7-1731-2007.

Cho, H.-K., and H.-Y. Chun (2008), Impacts on the TRMM data due to orbit boost in the spectral domain, *Geophys. Res. Lett.*, *35*, L01403, doi:10.1029/2007GL032320.

Claud, C., B. Alhammoud, B. M. Funatsu, and J.-P. Chaboureau (2010), Mediterranean hurricanes: Large-scale environment and convective and precipitating areas from satellite microwave observations, *Nat. Hazards Earth Syst. Sci.*, *10*, 2199–2213, doi:10.5194/nhess-10-2199-2010.

Claud, C., B. Alhammoud, B. M. Funatsu, C. Lebeaupin Brossier, J.-P. Chaboureau, K. Béranger, and P. Drobinski (2012), A high resolution climatology of precipitation and deep convection over the Mediterranean region from operational satellite microwave data: Development and application to the evaluation of model uncertainties, *Nat. Hazards Earth Syst. Sci.*, *12*, 785–798, doi:10.5194/nhess-12-785-2012.

Correia, F. W. S., R. C. S. Alvala, and A. O. Manzi (2008), Modeling the impacts of land cover change in Amazonia: A regional climate model (RCM) simulation study, *Theor. Appl. Climatol.*, *93*, 225–244, doi:10.1007/s00704-007-0335-z.

Costa, M. H., and G. F. Pires (2010), Effects of Amazon and central Brazil deforestation scenarios on the duration of the dry season in the arc of deforestation, *Int. J. Climatol.*, *30*, 1970–1979, doi:10.1002/joc.2048.

Costa, M. H., S. N. M. Yanagi, P. J. O. P. Souza, A. Ribeiro, and E. J. P. Rocha (2007), Climate change in Amazonia caused by soybean cropland expansion, as compared to caused by pastureland expansion, *Geophys. Res. Lett.*, *34*, L07706, doi:10.1029/2007GL029271.

Cox, P. M., R. A. Betts, C. D. Jones, S. A. Spall, and I. J. Totterdell (2000), Acceleration of global warming due to carbon-cycle feedbacks in a coupled climate model, *Nature*, *408*, 184–187, doi:10.1038/35041539.

Cox, P. M., R. A. Betts, M. Collins, P. P. Harris, C. Huntingford, and C. D. Jones (2004), Amazonian forest dieback under climate-carbon cycle

projections for the 21st century, *Theor. Appl. Climatol.*, *78*, 137–156, doi:10.1007/s00704-004-0049-4.

da Rocha, R. P., C. A. R. Morales, S. V. Cuandra, and T. Ambrizzi (2009), Precipitation diurnal cycle and summer climatology assessment over South America: An evaluation of Regional Climate Model version 3 simulations, *J. Geophys. Res.*, *114*, D10108, doi:10.1029/2008JD010212.

Davidson E. A., et al. (2012), The Amazon basin in transition, *Nature*, *481*, 321–328, doi:10.1038/nature10717.

Deeter, M. N., and J. Vivekanandan (2005), AMSU-B observations of mixed-phase clouds over land, *J. Appl. Meteorol.*, *44*, 72–85, doi:10.1175/JAM-2187.1.

Dessler, A. E. (2002), The effect of deep, tropical convection on the tropical tropopause layer, *J. Geophys. Res.*, *107*(D3), 4033, doi:10.1029/2001JD000511.

Dubreuil, V., R. Bariou, M. dos Passos, R. Ferrand, and V. Nedelec (2005), Evolution de la frontiere agricole dans le Centre Ouest du Mato Grosso: Municipes de Tangara da Serra, Campo Novo dos Parecis, Diamantino, *Cah. Agric.*, *124*, 217–224.

Dubreuil, V., A.-N. Laques, V. Nedelec, D. Arvor, and H. Gurgel (2008), Paysages et fronts pionniers amazoniens sous le regard des satellites: L'exemple du Mato Grosso, *Espace Geogr.*, *1*(37), 57–74.

Dubreuil, V., N. Debortoli, B. M. Funatsu, V. Nedelec, and L. Durieux (2012), Impact of land-cover change in the southern Amazonia climate: A case study for the region of Alta Floresta, Mato Grosso, Brazil, *Environ. Monit. Assess.*, *184*, 877–891, doi:10.1007/s10661-011-2006-x.

Durieux, L., L. A. T. Machado, and H. Laurent (2003), The impact of deforestation on cloud cover over the Amazon arc of deforestation, *Remote Sens. Environ.*, *86*, 132–140, doi:10.1016/S0034-4257(03)00095-6.

Durkee, J. D., and T. L. Mote (2010), A climatology of warm-season mesoscale convective complexes in subtropical South America, *Int. J. Climatol.*, *30*, 418–431, doi:10.1002/joc.1893.

Fearnside, P. M. (2002), Soybean cultivation as a threat to the environment in Brazil, *Environ. Conserv.*, *28*, 23–38.

Fearnside, P. M. (2005), Deforestation in Brazilian Amazonia: History, rates, and consequences, *Conserv. Biol.*, *19*, 680–688, doi:10.1111/j.1523-1739.2005.00697.x.

Ferraro, R. R., F. Weng, N. C. Grody, and L. Zhao (2000), Precipitation characteristics over land from the NOAA-15 AMSU sensor, *Geophys. Res. Lett.*, *27*, 2669–2672, doi:10.1029/2000GL011665.

Ferreira, S. A., and M. A. Gan (2011), Intraseasonal variability in the South American monsoon system, *Atmos. Sci. Lett.*, *12*, 253–260, doi:10.1002/asl.328.

Fu, R., and W. Li (2004), The influence of the land surface on the transition from dry to wet season in Amazonia, *Theor. Appl. Climatol.*, *78*, 97–110, doi:10.1007/s00704-004-0046-7.

Funatsu, B. M., C. Claud, and J.-P. Chaboureau (2007), Potential of Advanced Microwave Sounding Unit to identify precipitating systems and associated upper-level features in the Mediterranean region: Case studies, *J. Geophys. Res.*, *112*, D17113, doi:10.1029/2006JD008297.

Funatsu, B. M., C. Claud, and J.-P. Chaboureau (2008), A 6-year AMSU-based climatology of upper-level troughs and associated precipitation distribution in the Mediterranean region, *J. Geophys. Res.*, *113*, D15120, doi:10.1029/2008JD009918.

Funatsu, B. M., C. Claud, and J.-P. Chaboureau (2009), Comparison between the large scale environments of moderate and intense precipitating systems in the Mediterranean region, *Mon. Weather Rev.*, *137*, 3933–3959, doi:10.1175/2009MWR2922.1.

Gan, M. A., V. E. Kousky, and C. F. Ropelewski (2004), The South American monsoon circulation and its relationship to rainfall over west-central Brazil, *J. Clim.*, *17*, 47–66, doi:10.1175/1520-0442(2004)017<0047:TSAMCA>2.0.CO;2.

Gan, M. A., V. B. Rao, and M. C. L. Moscati (2005), South American monsoon indices, *Atmos. Sci. Lett.*, *6*, 219–223, doi:10.1002/asl.119.

Garcia-Carreras, L., and D. J. Parker (2011), How does local tropical deforestation affect rainfall?, *Geophys. Res. Lett.*, *38*, L19802, doi:10.1029/2011GL049099.

Greenwald, T. J., and S. A. Christopher (2002), Effect of cold clouds on satellite measurements near 183 GHz, *J. Geophys. Res.*, *107*(D13), 4170, doi:10.1029/2000JD000258.

Haddad, Z. S., E. A. Smith, C. D. Kummerow, T. Iguchi, M. R. Farrar, S. L. Durden, M. Alves, and W. S. Olson (1997a), The TRMM 'day-1' radar/radiometer combined rain-profiling algorithm, *J. Meteorol. Soc. Jpn.*, *75*, 799–809.

Haddad, Z. S., D. A. Short, S. L. Durden, E. Im, S. Hensley, M. B. Grable, and R. A. Black (1997b), A new parametrization of the rain drop size distribution, *IEEE Trans. Geosci. Remote Sens.*, *35*, 532–539, doi:10.1109/36.581961.

Hauf, T., P. Schulte, R. Alheit, and H. Schlager (1995), Rapid vertical transport by an isolated midlatitude thunderstorm, *J. Geophys. Res.*, *100*, 22,957–22,970, doi:10.1029/95JD02324.

Holton, J. R., and A. Gettelman (2001), Horizontal transport and dehydration of the stratosphere, *Geophys. Res. Lett.*, *28*, 2799–2802, doi:10.1029/2001GL013148.

Holton, J. R., P. H. Haynes, M. E. McIntyre, A. R. Douglass, R. B. Rood, and L. Pfister (1995), Stratosphere-troposphere exchange, *Rev. Geophys.*, *33*, 403–439, doi:10.1029/95RG02209.

Hong, G., G. Heygster, J. Miao, and K. Kunzi (2005), Detection of tropical deep convective clouds from AMSU-B vapour channels measurements, *J. Geophys. Res.*, *110*, D05205, doi:10.1029/2004JD004949.

Hong, G., G. Heygster, and C. A. M. Rodriguez (2006), Effect of cirrus clouds on the diurnal cycle of tropical deep convective clouds, *J. Geophys. Res.*, *111*, D06209, doi:10.1029/2005JD006208.

Hong, G., G. Heygster, J. Notholt, and S. A. Buehler (2008), Interannual to diurnal variations in tropical and subtropical deep convective clouds, *J. Clim.*, *21*, 4168–4189, doi:10.1175/2008JCLI1911.1.

Horel, J. D., A. N. Hahnmann, and J. C. Geisler (1989), An investigation of the annual cycle of convective activity over the tropical Americas, *J. Clim.*, *2*, 1388–1403.

Huntingford, C., et al. (2008), Towards quantifying uncertainty in predictions of Amazon 'dieback,' *Philos. Trans. R. Soc. B*, *363*, 1857–1864, doi:10.1098/rstb.2007.0028.

Iguchi, T., T. Kozu, R. Meneghine, J. Awaka, and K. Okamoto (2000), Rain-profiling algorithm for the TRMM precipitation radar, *J. Appl. Meteorol.*, *39*, 2038–2052, doi:10.1175/1520-0450(2001)040<2038:RPAFTT>2.0.CO;2.

Kikuchi, K., and B. Wang (2008), Diurnal precipitation regimes in the global tropics, *J. Clim.*, *21*, 2680–2696, doi:10.1175/2007JCLI2051.1.

Kleespies, T. J., and P. Watts (2006), Comparison of simulated radiances, Jacobians and linear error analysis for the Microwave Humidity Sounder and the Advanced Microwave Sounding Unit-B, *Q. J. R. Meteorol. Soc.*, *132*, 3001–3010, doi:10.1256/qj.05.03.

Koren, I., J. V. Martins, L. A. Remer, and H. Afargan (2008), Smoke invigoration versus inhibition of clouds over the Amazon, *Science*, *321*, 946–949, doi:10.1126/science.1159185.

Kousky, V. E., and M. T. Kagano (1981), A climatological study of the tropospheric circulation over the Amazon region, *Acta Amazon.*, *11*, 743–758.

Kubota, H., and T. Nitta (2001), Diurnal variations of tropical convection observed during the TOGA-COARE, *J. Meteorol. Soc. Jpn.*, *79*, 815–830, doi:10.2151/jmsj.79.815.

Kummerow, C., et al. (2000), The status of the tropical rainfall measuring mission (TRMM) after two years in orbit, *J. Appl. Meteorol.*, *39*, 1965–1982.

Kummerow, C. D., Y. Hong, W. S. Olson, S. Yang, R. F. Adler, J. McCollum, R. Ferraro, G. Petty, D. B. Shin, and T. T. Wilheit (2001), The evolution of the Goddard profiling algorithm (GPROF) for rainfall estimation from passive microwave sensors, *J. Appl. Meteorol.*, *40*, 1801–1820, doi:10.1175/1520-0450(2001)040<1801:TEOTGP>2.0.CO;2.

Lee, J.-E., B. R. Lintner, C. K. Boyce, and P. J. Lawrence (2011), Land use change exacerbates tropical South American drought by sea surface temperature variability, *Geophys. Res. Lett.*, *38*, L19706, doi:10.1029/2011GL049066.

Lenters, J. D., and K. H. Cook (1997), On the origin of the Bolivian High and related circulation features of the South American climate, *J. Atmos. Sci.*, *54*, 656–678, doi:10.1175/1520-0469(1997)054<0656:OTOOTB>2.0.CO;2.

Lepers, E., E. Lambin, A. Janetos, R. DeFries, F. Achard, N. Ramankutty, and R. Scholes (2005), A synthesis of information on rapid land-cover change for the period 1981–2000, *BioScience*, *55*, 115–124, doi:10.1641/0006-3568(2005)055[0115:ASOIOR]2.0.CO;2.

Lima, W. F. A., L. A. T. Machado, C. A. Morales, and N. Viltard (2007), Rainfall sensitivity analyses for the HSB sounder: An Amazon case study, *Int. J. Remote Sens.*, *28*, 3529–3545, doi:10.1080/01431160601013526.

Lin, J. C., T. Matsui, R. A. Pielke Sr., and C. Kummerow (2006), Effects of biomass-burning-derived aerosols on precipitation and clouds in the Amazon Basin: A satellite-based empirical study, *J. Geophys. Res.*, *111*, D19204, doi:10.1029/2005JD006884.

Malhi, Y., J. T. Roberts, R. A. Betts, T. J. Killeen, W. Li, and C. A. Nobre (2008), Climate change, deforestation, and the fate of the Amazon, *Science*, *319*, 169–172, doi:10.1126/science.1146961.

Marengo, J. A. (2004), Interdecadal variability and trends of rainfall across the Amazon basin, *Theor. Appl. Climatol.*, *78*, 79–86, doi:10.1007/s00704-004-0045-8.

Marengo, J. A., J. Tomasella, L. M. Alves, W. R. Soares, and D. A. Rodriguez (2011), The drought of 2010 in the context of historical

droughts in the Amazon region, *Geophys. Res. Lett.*, *38*, L12703, doi:10.1029/2011GL047436.

Morton, D., R. DeFries, Y. Shimabukuro, L. Anderson, E. Arai, F. del Bon Espirito-Santo, R. Freitas, and J. Morisette (2006), Cropland expansion changes deforestation dynamics in the southern Brazilian Amazon, *Proc. Natl. Acad. Sci. U. S. A.*, *103*, 14,637–14,641, doi:10.1073/pnas. 0606377103.

Nielsen, J. K., M. Foster, and A. Heidinger (2011), Tropical stratospheric cloud climatology from the PATMOS-x dataset: An assessment of convective contributions to stratospheric water, *Geophys. Res. Lett.*, *38*, L18801, doi:10.1029/2011GL049429.

Nishizawa, T., and M. Tanaka (1983), The annual change in the tropospheric circulation and the rainfall in South America, *Meteorol. Atmos. Phys.*, *33*, 107–116, doi:10.1007/BF02273994.

Nobre, C. A., and L. D. S. Borma (2009), 'Tipping points' for the Amazon forest, *Curr. Opin. Environ. Sustainability*, *1*, 28–36, doi:10.1016/j.cosust.2009.07.003.

Nobre, C. A., P. J. Nobre, and J. Shukla (1991), Amazonian deforestation and regional climate change, *J. Clim.*, *4*, 957–988, doi:10.1175/1520-0442(1991)004<0957:ADARCC>2.0.CO;2.

Ohsawa, T., H. Ueda, T. Hayashi, A. Watanabe, and J. Matsumoto (2001), Diurnal variation of convective activity and rainfall in tropical Asia, *J. Meteorol. Soc. Jpn.*, *79*, 333–352, doi:10.2151/jmsj.79.333.

Oyama, M. D., and C. A. Nobre (2003), A new climate-vegetation equilibrium state for tropical South America, *Geophys. Res. Lett.*, *30*(23), 2199, doi:10.1029/2003GL018600.

Pielke, R. A. (2001), Influence of the spatial distribution of vegetation and soils on the prediction of cumulus convective rainfall, *Rev. Geophys.*, *39*, 151–177, doi:10.1029/1999RG000072.

Pongratz, J., L. Bounoua, R. S. DeFries, D. C. Morton, L. O. Anderson, W. Mauser, and C. A. Klink (2006), The impact of land cover change on surface energy and water balance in Mato Grosso, Brazil, *Earth Interact.*, *10*, 1–17, doi:10.1175/EI176.1.

Ramos da Silva, R., D. Werth, and R. Avissar (2008), Regional impacts of future land-cover changes on the Amazon Basin wet-season climate, *J. Clim.*, *21*, 1153–1170, doi:10.1175/2007JCLI1304.1.

Roy, S. B., and R. Avissar (2002), Impact of land use/land cover change on regional hydrometeorology in Amazonia, *J. Geophys. Res.*, *107*(D20), 8040, doi:10.1029/2000JD000263.

Sampaio, G., C. Nobre, M. H. Costa, P. Satyamurty, B. S. Soares-Filho, and M. Cardoso (2007), Regional climate change over eastern Amazonia caused by pasture and soybean cropland expansion, *Geophys. Res. Lett.*, *34*, L17709, doi:10.1029/2007GL030612.

Silva Dias, M. A. F., et al. (2002), Cloud and rain processes in a biosphere-atmosphere interaction context in the Amazon region, *J. Geophys. Res.*, *107*(D20), 8072, doi:10.1029/2001JD000335.

Siqueira, J. R., and L. A. T. Machado (2004), Influence of the frontal systems on the day to day convection variability over South America, *J. Clim.*, *17*, 1754–1766, doi:10.1175/1520-0442(2004)017<1754: IOTFSO>2.0.CO;2.

Surussavadee, C., and D. H. Staelin (2010), Global precipitation retrievals using the NOAA AMSU millimeter-wave channels: Comparisons with rain gauges, *J. Appl. Meteorol. Climatol.*, *49*, 124–135, doi:10.1175/2009JAMC2262.1.

Tian, B., B. J. Soden, and X. Wu (2004), Diurnal cycle of convection, clouds, and water vapour in the tropical upper troposphere: Satellites versus a general circulation model, *J. Geophys. Res.*, *109*, D10101, doi:10.1029/2003JD004117.

Virji, H. (1981), A preliminary study of summertime tropospheric circulation patterns over South America estimated from cloud winds, *Mon. Weather Rev.*, *109*, 599–610, doi:10.1175/1520-0493(1981)109<0599: APSOST>2.0.CO;2.

von Randow, C., et al. (2004), Comparative measurements and seasonal variations in energy and carbon exchange over forest and pasture in south west Amazonia, *Theor. Appl. Climatol.*, *78*, 5–26, doi:10.1007/s00704-004-0041-z.

Walker, R., N. J. Moore, E. Arima, S. Perz, C. Simmons, M. Cladas, D. Vergara, and C. Bohrer (2009), Protecting the Amazon with protected areas, *Proc. Natl. Acad. Sci. U. S. A.*, *106*, 10,582–10,586, doi:10.1073/pnas.0806059106.

Wang, C., and J. Chang (1993), A three-dimensional numerical model of cloud dynamics, microphysics, and chemistry: 3. Redistribution of pollutants, *J. Geophys. Res.*, *98*, 16,787–16,798, doi:10.1029/93JD01865.

Wang, G., S. Sun, and R. Mei (2011), Vegetation dynamics contributes to the multi-decadal variability of precipitation in the Amazon region, *Geophys. Res. Lett.*, *38*, L19703, doi:10.1029/2011GL049017.

Wang, P. K., M. Setvák, W. Lyons, W. Schmid, and H.-M. Lin (2009), Further evidences of deep convective vertical transport of water vapor through the tropopause, *Atmos. Res.*, *94*, 400–408, doi:10.1016/j.atmosres.2009.06.018.

Weng, F., L. Zhao, R. R. Ferraro, G. Poe, X. Li, and N. Grody (2003), Advanced microwave sounding unit cloud and precipitation algorithms, *Radio Sci.*, *38*(4), 8068, doi:10.1029/2002RS002679.

Yoshikawa, S., and K. Sanga-Ngoie (2011), Deforestation dynamics in Mato Grosso in the southern Brazilian Amazon using GIS and NOAA/AVHRR data, *Int. J. Remote Sens.*, *32*, 523–544, doi:10.1080/01431160903475225.